Pyrolysis of 2-methoxy-2,3,3-trimethylbutane (MTMB) monitored by 118 nm photoionization mass spectrometry

Kevin Weber [a], Jingsong Zhang [a,b], Dan Borchardt [a], Thomas Hellman Morton [a,*]

[a] *Department of Chemistry, University of California, Riverside, CA 92521-0403, United States*
[b] *Air Pollution Research Center, University of California, Riverside, CA 92521-0424, United States*

In memoriam Chava Lifshitz

Abstract

Pyrolysis/supersonic jet expansion/118.2 nm photoionization TOF mass spectrometry is used to examine competitive thermal dissociations of a deuterated analogue of the title compound, a potential antiknock additive for motor fuel. At high temperatures neutral $(CH_3)_3CC(CD_3)_2OCH_3$ (MTMB-d_6) undergoes homolytic cleavage of its 2,3-bond in competition with molecular elimination of methanol. G3X and CCSD calculations predict the dissociation energy of this bond to differ only slightly from that of the 2,3-bond in hexamethylethane (HME). Theory also predicts that the 2,3-bond is the weakest bond of MTMB. Pyrolysis of MTMB-d_6 below 1000 K shows no production of CD_3 radicals, but only methyl and *tert*-butyl radicals, along with acetone-d_6 and the products from molecular elimination of methanol. While MTMB-d_6 exhibits desirable solubility characteristics in water (relative to the presently used fuel oxygenates MTBE and TAME), the predominance of bond homolysis at temperatures >900 K suggests (according to one current model for how fuel oxygenates inhibit autoignition) that MTMB ought to exhibit poor antiknock characteristics.

1. Introduction

tert-Alkyl methyl ethers have seen wide use as fuel additives for nearly 40 years. As replacements for tetraethyllead, the simplest homologues – methyl *tert*-butyl ether (MTBE) and *tert*-amyl methyl ether (TAME) – present a new set of problems. Because of their water solubility, leakage from underground storage tanks and pipelines threatens to contaminate the water table with volatile compounds that can be smelled at part per billion concentrations [1].

Higher homologues have been discussed as alternatives to MTBE and TAME, because they are expected to be much less soluble in water. More highly branched methyl ethers have attracted particular attention. *tert*-Octyl methyl ether (2-methoxy-2,4,4-trimethylpentane, TOME) exhibits excellent antiknock properties [2], and approaches to its large scale pro-

duction have recently been described [3]. Several patents and procedures outline the preparation and utilization of *tert*-hexyl methyl ether (2-methoxy-2,3-dimethylbutane, MDMB) along with other homologues and isomers [4–9].

Conspicuously absent from this literature is the most highly branched example, 2-methoxy-2,3,3-trimethylbutane, which will be abbreviated below as MTMB. While general discussions of replacements for MTBE allude to this compound, very little specific information has been provided [4,9]. MTMB has been the focus of NMR studies of internal rotation [10], because of its high degree of internal steric hindrance, and has recently been studied (along with TAME, MDMB, TOME, and other homologues) by photoionization mass spectrometry [11]. However, the thermal decomposition of the neutral compound has not been discussed heretofore.

Two aspects of oxygenated fuel additives have become of paramount interest. The first is their antiknock activity in an automobile motor. The second is their solubility in water. Engine knock results from explosion of the fuel–oxygen mixture in front of the flame front during the power stroke [12]. If the fuel–air

mixture at the far end of a hot cylinder ignites before the flame initiated by the sparkplug arrives, damage to the motor can result (not to mention loss of power and inefficient use of fuel). A definitive mechanism for the action of antiknock agents has not been described in the open literature, but there is no shortage of published hypotheses [2]. The behavior of oxygenated compounds at high temperatures provides a guide to how a compound might function when it comes in contact with a hot cylinder wall.

The second aspect addresses the fate of fuel that finds its way into the environment. Partition of fuel oxygenates into ground water has caused considerable alarm, regardless of whether they actually inflict environmental damage or have serious health effects. This paper addresses both aspects: the water solubilities of MDMB, MTMB, and TOME are compared with those of TAME and MTBE, and the primary thermal decomposition channels of neutral MTMB at high temperatures are described, as monitored by photoionization mass spectrometry.

Traditional kinetic studies of bond homolyses have made use of scavenger techniques [13,14], in order to assess the extent to which free radicals are formed. These methods examine the stable products derived from free radicals, rather than observing the radicals directly. In recent years, photoionization mass spectrometry has become a useful technique for interrogating free radicals [15,16]. In order for this approach to work, products of bond homolysis must give spectroscopic signatures that differ from those of the reactants or the products from other pathways. One of the most characteristic signatures is that of methyl cation (m/z 15), which arises uniquely from methyl radical at low photon energies. In the present study, 118 nm photoionization of the pyrolysis products of deuterated MTMB reveals the formation of methyl radicals, along with other products that are characteristic of bond homolysis.
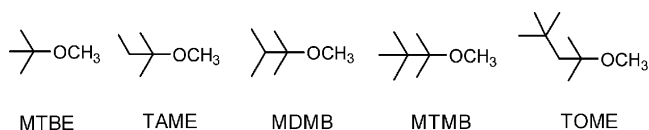
The approach in these experiments presents several advantages: (1) a short reaction time to examine the initial steps of the thermal decomposition; (2) supersonic cooling, which quenches the reaction and minimizes recombination of products and intermediates; (3) minimal ion fragmentation by the use of the 10.48 eV "soft" photoionization source that imparts sufficient energy to ionize many closed-shell and free radical species. The supersonic cooling further reduces photoionization fragmentation by minimizing the internal energy of the parent molecules and the pyrolysis products.

Previous work from these laboratories has dealt with thermal decomposition of MTBE [16]. Molecular elimination represents the predominant mechanism, as Scheme 1 portrays. The published Arrhenius activation parameters ($E_a = 247 \pm 4$ kJ mol^{-1}; $A = 10^{13.9}$ s^{-1}) [17] correspond to dissociation of MTBE into methanol and isobutene, as the upper pathway in Scheme 1 depicts for an isotopically labeled analogue.

As we have previously reported in this journal, bond homolysis begins to compete with elimination at temperatures ≥ 1000 K [16]. While the thermodynamic threshold for homolysis is much
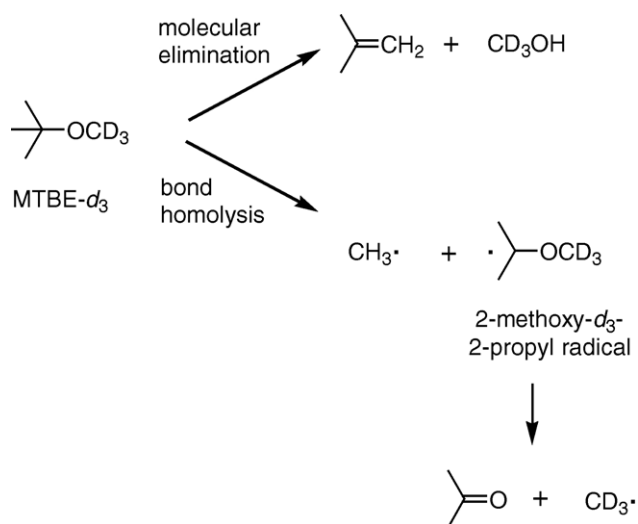
Scheme 1.

higher than the E_a for molecular elimination, the Arrhenius pre-exponential factors for bond homolyses are also much larger ($A > 10^{16}$ s^{-1} [17]). Consequently, at suitably high temperatures molecular elimination and homolysis proceed with comparable rates. As in the case of most thermal decomposition experiments with neutral molecules (except those performed in shock tubes or "wall-less reactors" [17]), it is difficult to rule out surface catalysis. However, the observed behavior is consistent with the activation parameters for homogeneous gas phase reactions.

Bond homolysis of MTBE initially forms a methyl radical and a 2-methoxy-2-propyl radical, as illustrated by the lower pathway in Scheme 1. The 2-methoxy-2-propyl radical is unstable under the reaction conditions and dissociates to acetone plus a second methyl radical. Hence, bond homolysis of the deuterated MTBE shown in Scheme 1 yields a d_3-methyl radical and an undeuterated methyl radical, along with a molecule of acetone. At higher temperatures, acetone itself undergoes bond homolysis to produce acetyl radical and, ultimately, to yield two methyl radicals and carbon monoxide.

TOME undergoes the same sort of molecular elimination as does MTBE [16]. In those experiments, though, further decomposition of the olefinic products obscured the radicals that would be expected from bond homolysis. Thus, it remains unclear whether the competition represented in Scheme 1 operates at elevated temperatures for the higher homologues of MTBE. Results presented here for MTMB show that homolysis competes effectively with molecular elimination in the case of this homologue.

2. Experimental

Thermal decomposition experiments were performed in an apparatus that has previously been described [16], which uses a Wiley–MacLaren type linear time-of-flight mass spectrometer to monitor pyrolysis products by means of 118 nm photoionization. The main reaction chamber is pumped by a cryobaffled
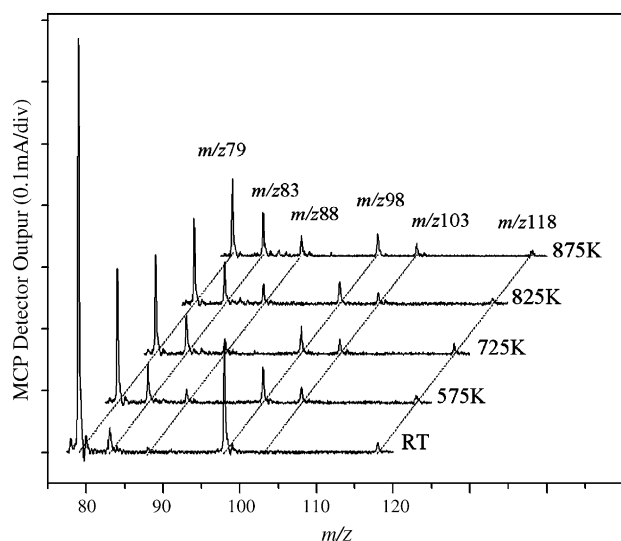
Fig. 1. Stack plot of pyrolysis/supersonic jet expansion/118.2 nm photoionization TOF mass spectra of MTMB-d_6 seeded in argon (with a small amount of 2,3,3-trimethyl-2-butene as internal standard) as a function of nozzle temperature.

Fig. 2. Stack plot of pyrolysis/supersonic jet expansion/118.2 nm photoionization TOF mass spectra of MTMB-d_6 seeded in helium (with a small amount of MTBE as internal standard) as a function of nozzle temperature.

Varian VHS-6 diffusion pump, and the mass spectrometer is differentially pumped with a turbomolecular pump and a liquid nitrogen trap. Pyrolyses are carried out by expanding the parent molecules, seeded in helium or argon, via a heated silicon carbide tube through a pulsed valve into the photoionization region of the mass spectrometer, similar to apparatus described by Chen and coworkers [19]. A 1 mm i.d. silicon carbide tube (1 mm i.d. and 2 mm o.d.) is attached to a machinable piece of alumina mounted to the faceplate of the pulsed valve by means of a high-temperature, ceramic adhesive. The alumina piece has a 2 mm i.d. channel to allow the gas flow from the pulsed valve to the silicon carbide tube, and it insulates the silicon carbide tube (2 mm o.d.) both thermally and electrically from the pulsed valve. Two graphite electrodes press-fitted onto the silicon carbide tube are resistively heated, with electrical current controlled by a Variac transformer. Nominal temperature is monitored with a type C thermocouple (Omega) wrapped around the outside of the heated portion of the silicon carbide nozzle. The temperature calibration curve was plotted by inserting a thermocouple insulated with ceramic adhesive into the heated nozzle and comparing that reading ($T_{internal}$) with the nominal temperature ($T_{nominal}$), which gives the empirical relation $T_{internal}$ (in °C) = $1.38 T_{nominal} - 200$ °C for $T_{nominal} \geq 400$ °C. Heat dissipation by the inserted thermocouple may have a greater cooling effect than the gas pulse, so the calibration equation represents only a best approximation, and the nominal temperatures are reported in Figs. 1–3 to the nearest 25°. With a near-sonic velocity of the sample within the nozzle, the residence time in the heater has been estimated to be approximately 20 μs when helium is the carrier gas [19]. Assuming that the sonic velocity scales with the square root of mass (and neglecting viscosity and other additional effects), the residence time when argon is the carrier gas should be >3 times longer.

After exiting from the heated zone the unreacted precursor and its products are cooled by supersonic expansion. The degree
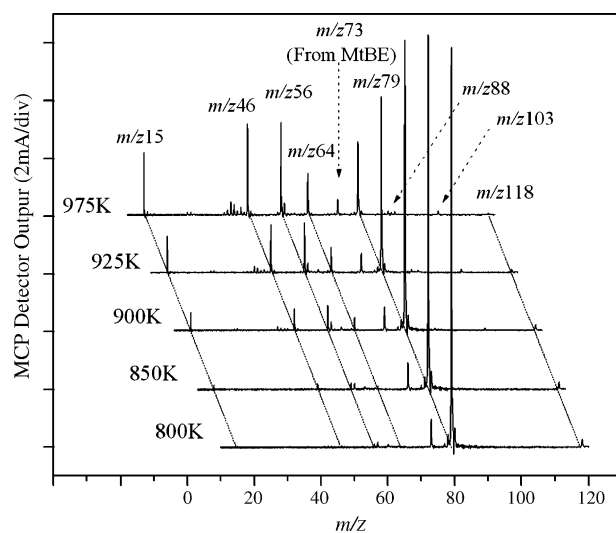

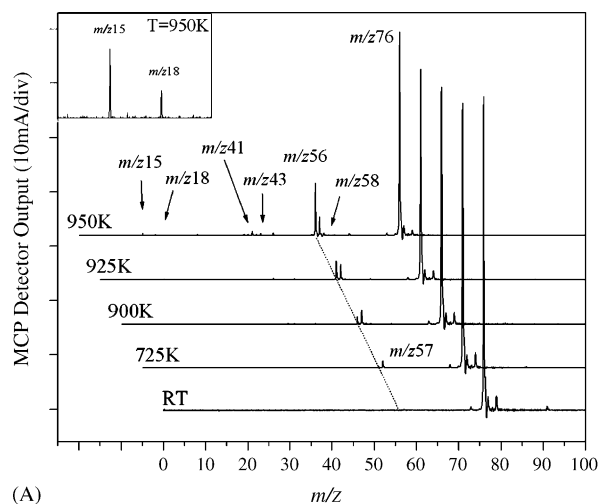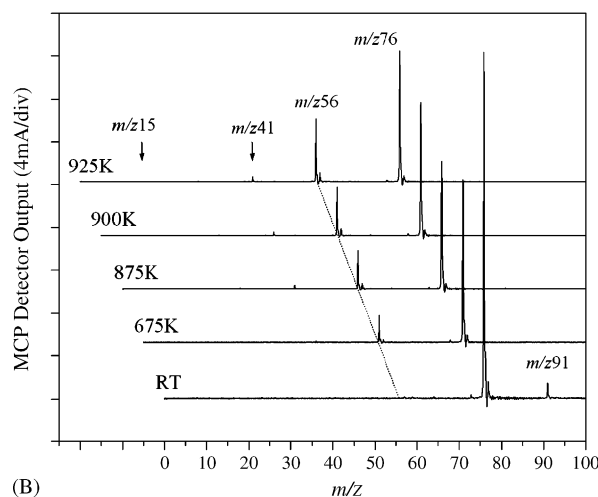Fig. 3. Stack plots of pyrolysis/supersonic jet expansion/118.2 nm photoionization TOF mass spectra of MTBE-d_3 seeded in helium (A, with inset showing low mass fragments at 950 K, intensity 40×) and argon (B) as functions of nozzle temperature.

Table 1
Solubilities of *tert*-alkyl methyl ethers in water at 20 °C

Formula	Abbreviated	Molarity (mM)	mg/l
$(CH_3)_3COCH_3$	MTBE[a]	403	3.55×10^4
$CH_3CH_2C(CH_3)_2OCH_3$	TAME[b]	110	1.1×10^4
$(CH_3)_2CHC(CH_3)_2OCH_3$	MDMB[c]	19	2200
$(CH_3)_3CC(CH_3)_2OCH_3$	MTMB[c]	1.4	180
$(CH_3)_3CCH_2C(CH_3)_2OCH_3$	TOME[c]	0.6	90

[a] Ref. [29].
[b] Ref. [30].
[c] This work.

Scheme 2.

of cooling increases with the mass of the carrier gas, and the rotational temperature of molecules in the jet after expansion is ≤50 K, as has been ascertained by Chen and coworkers [20] by means of multiphoton ionization (although the vibrational temperature tends to be somewhat higher).

Samples are introduced into the pyrolysis apparatus with the carrier gas (helium or argon, pressure at 950 Torr) bubbled through the samples. Pyrolysis products are ionized by single photon ionization at 118.2 nm (10.48 eV) using the frequency tripled third harmonic (355 nm) of an Nd:YAG laser output in a low pressure (30 Torr) Xe cell attached directly to the vacuum chamber. The 118.2 nm light is focused into the ionization chamber using an MgF_2 lens. The photoion current was detected using a microchannel plate (MCP) detector, which amplifies current by approximately 6 log units.

MTBE-d_3 was purchased from Cambridge Isotope Laboratories, acetone-$d6$ from Aldrich Chemical Co., and 2,3,3-trimethyl-2-butene from ChemSampCo; these commercial products were used without further purification. Methoxy-2,3,3-trimethylbutane-d_6 (MTMB-d_6) was prepared as previously described [11] by addition of excess acetone-d_6 to a pentane solution of *tert*-butyllithium at −78° C followed by distillation of the recovered alcohol and conversion to the methyl ether in THF solution. The product ether was twice distilled at atmospheric pressure (bp 118–121 °C). Other deuterated *tert*-alkyl methyl ethers were prepared in similar fashion, as previously described [11,16].

Water solubilities of deuterated *tert*-alkyl methyl ethers were determined using ^{2}H NMR. An excess of the ether was sealed in a glass ampoule with deionized water, repeatedly mixed by shaking, and allowed to stand for at least 24 h. The NMR spectrum of the aqueous layer was recorded and the peaks from CD_3 groups integrated relative to the natural abundance HOD peak (which was taken to be 16.7 mM).

3. Results

The impetus for studying multiply branched *tert*-alkyl methyl ethers derives from the water solubility of MTBE. As Table 1 summarizes, TAME (the replacement presently in use) is about one-third as soluble as MTBE on a mass basis. Further branching causes a sharp decrease in water solubility, as tabulated for MDMB, MTMB, and TOME. The biggest drop (more than a factor of 10) occurs with the increase in branching in going from
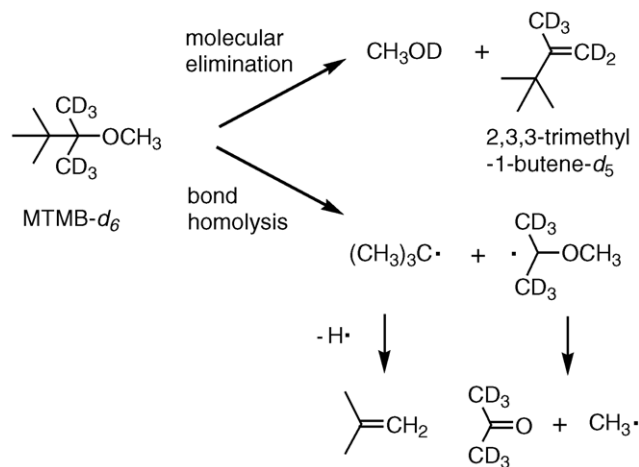
MDMB to MTMB. On a mass basis, MTMB is nearly 200 times less soluble than MTBE, while TOME is 400 times less soluble than MTBE.

Scheme 2 illustrates the products expected from gas phase pyrolysis of MTMB-d_6. Molecular elimination of CH_3OD should yield 2,3,3-trimethyl-1-butene-d_5, as shown. Homolysis of the weakest bond of MTMB-d_6 ought to produce *tert*-butyl radical and a deuterated 2-methoxy-2-propyl radical. Both of those radicals should dissociate further under the reaction conditions. The *tert*-butyl radical is known to expel a hydrogen atom at elevated temperatures: the published kinetic parameters predict it should have a lifetime on the order of 10^{-6} s at 1000 K [21]. As noted above, the 2-methoxy-2-propyl radical is also unstable: the deuterated analogue should dissociate to methyl radical plus acetone-d_6.

The thermal decomposition of MTMB-d_6 was performed by seeding the sample both in argon and in helium passed through the pyrolysis tube, followed by supersonic expansion and 118 nm photoionization. With a heavier carrier gas, contact time is increased, while the jet expansion gives more effective vibrational cooling. The mass spectra of a sample in argon pyrolyzed in the temperature domain 575–900 K is shown in Fig. 1, in which a small amount of unlabeled 2,3,3-trimethyl-1-butene was included for comparison. For clarity, only the region above m/z 77 is shown in Fig. 1. The bottom trace shows the mass spectrum of a room temperature sample cooled by supersonic jet expansion. Note that the base peak intensities (m/z 79 from MTMB and m/z 98 from the added alkene) drop sharply in going from room temperature to 575 K. This is a consequence of the decrease in number density of the sample when it is heated.

Undeuterated 2,3,3-trimethyl-1-butene was examined separately as well as in a mixture with MTMB-d_6. Photoionization of this alkene produces two ions, m/z 98 (the molecular ion) and m/z 83, the M-CH_3 fragment ion. No m/z 15 ion is seen below 850 K, which confirms that m/z 83 results from mass spectrometric decomposition of ionized 2,3,3-trimethyl-1-butene, rather than bond homolysis prior to ionization. At higher temperatures the m/z 83 intensity becomes larger than that of m/z 98, as bond

homolysis of the neutral alkene starts to produce the allylic radical $(CH_3)_2C=C(CH_3)CD_2^{\bullet}$ (and m/z 15 begins to appear).

The ions at m/z 103 and m/z 88 in Fig. 1 correspond to 2,3,3-trimethyl-1-butene-d_5 (from molecular elimination) and its M-CH$_3$ fragment. The ions at m/z 79 and m/z 118 come from the intact starting material: $(CD_3)_2C=OCH_3^{+}$, the M-(CH$_3$)$_3$C ion from MTMB-d_6, and $(CH_3)_3CC(CD_3)=OCH_3^{+}$, the M-CD$_3$ ion from MTMB-d_6 [11]. The extent of molecular elimination is comparable to what is observed for MTBE in this temperature domain. Methanol cannot be detected in these experiments because its IE is higher than 10.48 eV [21]. Fragments lighter than m/z 79 are not seen below 850 K with argon as carrier gas.

Pyrolyses of samples of MTMB-d_6 seeded in helium are summarized by the stack plot of photoionization mass spectra in Fig. 2. The carrier gas was changed in order to shorten the contact time, so as to minimize the contribution from pyrolysis of the alkene from molecular elimination. At 800 K, in addition to the fragment ions from MTMB-d_6 (which does not exhibit a molecular ion), there is a peak at m/z 73 from a trace of MTBE ($(CH_3)_2C=OCH_3^{+}$, the M-CH$_3$ ion from MTBE), which was added to facilitate mass calibration. The molecular ion of MTBE is too weak to detect under these conditions [16], while MTMB-d_6 exhibits no molecular ion at all.

As the temperature of the pyrolysis tube is raised above 850 K, six new ions appear: m/z 15, m/z 46, m/z 56, m/z 57, m/z 64, as well as a very small m/z 88 peak. The lightest of these is methyl cation, which comes from photoionization of methyl radical. It is significant that no m/z 18 (CD$_3^{+}$) emerges until much higher temperatures. The heaviest ion corresponds to photoionization of 2,3,3-trimethyl-2-butene-d_5 and of the allylic ion, $(CH_3)_2C=C(CD_3)CD_2^{\bullet}$, from its pyrolysis. The m/z 64 ion is the molecular ion from photoionization of the acetone-d_6 product, and m/z 46 is its M-CD$_3$ fragment. Photolysis of an authentic sample of acetone-d_6 in the experimental apparatus shows that the m/z 46 fragment always accompanies the molecular ion, providing a distinctive signature. Finally, m/z 57 comes from photoionization of the *tert*-butyl radical, while m/z 56 comes from photoionization of isobutene, the olefin produced by loss of a hydrogen atom from *tert*-butyl radical (as portrayed in Scheme 2) [18]. The growth of the m/z 15, 46, 56, 57, and 64 peak intensities with increasing temperature demonstrates the dominance of the homolysis channel shown in Scheme 2.

The m/z 88 ion from 2,3,3-trimethyl-2-butene-d_5 has a very low intensity above 850 K. At this temperature, 2,3,3-trimethyl-2-butene does begin to dissociate; the neutral alkene undergoes bond scission to $(CH_3)_2C=C(CD_3)CD_2^{\bullet}$ and methyl radical. From the control experiments on pyrolysis of the neutral, undeuterated alkene, however, it is clear that the m/z 15 peak seen in the MTMB-d_6 pyrolysis arises via the homolysis depicted in Scheme 2, rather than by dissociation of the alkene subsequent to molecular elimination.

The relative ion intensities in Fig. 2 imply that molecular elimination (for which the signal occurs at m/z 88) is a minor pathway above 900 K. For purposes of comparison, the stack plots in Fig. 3 summarize the dissociation of MTBE-d_3 in the same temperature domain. Isobutene (m/z 56) is the principal product from MTBE. As the intensity of m/z 56 increases with

temperature, the photofragment at m/z 41 becomes visible (as confirmed by examination of an authentic sample of isobutene under the same conditions). As previously described, m/z 43 comes from thermal decomposition of acetone [16], a product of the bond homolysis drawn in Scheme 1.

The pyrolysis/photoionization mass spectra in Fig. 3 illustrate an additional complication in interpreting experimental results. Supersonic expansion in helium cools a room temperature sample down to <50 K. Expansion of much hotter sample gives a jet with a correspondingly higher vibrational temperature. Some compounds show photoionization mass spectra that exhibit great sensitivity to vibrational energy content. MTBE is a case in point. An ion at m/z 57 appears upon heating, at temperatures below the onset of thermal decomposition, as indicated by its intensity relative to m/z 56 at 725 K in Fig. 3A. That ion contributes an intense peak in the published EI mass spectrum of MTBE at room temperature [21], but this mass spectrometric fragmentation is effectively suppressed by cooling in a supersonic jet. When the temperature of the sample in the jet is elevated, the fragmentation of ionized MTBE to m/z 57 comes back.

One way of probing the temperature dependence of the photoionization mass spectrum is to examine supersonic expansions in argon carrier gas, which provides more effective cooling. Fig. 3A and B compare the pyrolysis/photoionization results of MTBE-d_3 for these carrier gases. At room temperature, expansion of MTBE-d_3 in argon leads to a visible molecular ion peak at m/z 91. Expansion in helium gives a much smaller molecular ion peak, which is barely detectable. As noted above, MTBE-d_3 gives rise to m/z 57 ion when it is heated prior to super-sonic expansion in helium, even when no thermal decomposition is taking place. By contrast, pyrolysis/photoionization using argon as carrier gas gives greatly reduced intensities of m/z 57.

Following supersonic cooling, acetone, MTMB-d_6, and 2,3,3-trimethyl-2-butene display much less dependence of their photoionization mass spectra upon vibrational energy content (at least, as can be assessed by comparing expansion in helium versus argon). Thus the following inferences may be drawn:

(1) Comparison of Fig. 1 with Fig. 3B indicates that molecular elimination from MTMB-d_6 (as signaled by m/z 103 and its m/z 88 fragment ion) and MTBE-d_3 (as signaled by m/z 56) exhibit similar dependence upon pyrolysis temperature: alkene peaks become apparent around 600 K. In Fig. 1 the m/z 88 and m/z 103 peak intensities at 875 K add up to about 40% of the intensity of m/z 79, while in Fig. 3B the m/z 56 peak at 875 K has an intensity 30% that of m/z 76.

(2) The onset of bond homolysis of MTBE-d_3 in helium begins to be detectable at 950 K (Fig. 3A), at which temperature m/z 15 and m/z 18 are both seen, as expected on the basis of Scheme 1 (some additional m/z 15 comes from thermal decomposition of acetone at this temperature).

(3) In helium, the peaks characteristic of homolysis of MTMB-d_6 – m/z 15, m/z 46 and 64, and m/z 56 and 57 (as expected on the basis of Scheme 2) – begin to appear at 850 K. Under these conditions the peaks corresponding to molecular elimination – m/z 88 and 103 – cannot be seen until above 900 K

and never become as intense as the peaks from bond homolysis.

Taking carrier gas effects into consideration, we conclude that homolytic bond cleavage of MTMB-d_6 overtakes molecular elimination as the predominant thermal dissociation pathway around 900 K.

4. Calculations

Two thermal decomposition precedents can be compared with the results for MTMB. The homogeneous gas phase cleavage of hexamethylethane (HME; X = Y = CH$_3$ in Eq. (1)) has been closely studied [13]. Thermal cleavages of the dimethyl ethers of tertiary *vic*-diols have also been examined [14]. While the simplest example, pinacol dimethyl ether (PDME; X = Y = OCH$_3$ in Eq. (1)), has not been reported, extrapolation from its higher homologues predicts an activation energy approximately 45–50 kJ mol^{-1} lower than that of HME. Homolyses of HME and of tertiary *vic*-diol dimethyl ethers are reported to have Arrhenius preexponential factors on the order of 10^{17} s^{-1}. It is not obvious a priori whether cleavage of the central bond of MTMB should be much easier than that of HME (as it is for PDME). This question has been addressed by means of computation.

HME: X=Y=CH$_3$
PDME: X=Y=OCH$_3$
MTMB: X=CH$_3$, Y=OCH$_3$ (1)
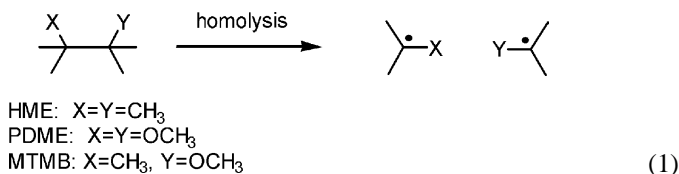
Computations were explored using three levels of theory using the GAUSSIAN98 and GAUSSIAN03 program suites, all based on geometries optimized using density functional theory (DFT) at B3LYP/6-31(2df,p): DFT, G3X, and coupled clusters (CCSD) using single and double excitations. G3X theory represents a composite approach; it makes use of DFT zero point energies (scaled by a factor of 0.9854) and single-point electronic energies calculated at several higher ab initio levels. The G3X energy is determined by sums and differences of those single-point energies, including the scaled zero point energy and a higher level correction [22,23]. In the case of HME, DFT optimization with no symmetry constraint gives the lowest electronic energy, but the geometry with D_{3d} symmetry possesses a lower zero point energy, which makes the D_{3d} structure energetically more favorable. MTMB was optimized with no symmetry constraint, while MTBE and the methoxythexyl radical (MeOCMe$_2$CMe$_2^\bullet$) preferred C_s symmetry. Methyl and *tert*-butyl radicals were optimized with C_{3v} symmetry constraints, but no constraint was imposed in the optimization of 2-methoxyisopropyl radical (MeOCMe$_2^\bullet$) or *t*BuCMeOMe$^\bullet$. Table 2 summarizes the results calculated for homolyses of HME, MTMB, and MTBE.

At the DFT level the 0 K bond dissociation energy (D_0) of HME is calculated to be 246 kJ mol^{-1}, considerably lower than the reported experimental 300 K bond dissociation energy of 322 kJ mol^{-1} [24]. Consideration of basis set superposition error (which is neglected here) would lower the calculated DFT value even further. By contrast, G3X theory predicts a D_0 value of 332 kJ mol^{-1} for HME, while CCSD gives a value of $D_0 = 313$ kJ mol^{-1} when unscaled zero point energies are taken into account.

G3X theory gives a 0 K bond dissociation energy for the central bond of MTMB of $D_0 = 330$ kJ mol^{-1}, while CCSD predicts a value of 316 kJ mol^{-1}. That is to say, both computational levels predict the homolyses of the 2,3-bonds of HME and MTMB in Eq. (1) to have nearly the same endothermicities. The value for homolysis of a methyl radical off of the *tert*-butyl group of MTMB (the 3,4-bond) to form a methoxythexyl radical (MeOCMe$_2$CMe$_2^\bullet$) is much higher, for which G3X theory predicts $D_0 = 354$ kJ mol^{-1}.

G3X and CCSD give quite different estimates of the enthalpy changes for cleavage of α-methyl groups. For homolysis of the 1,2-bond of MTBE (breaking apart the *tert*-butyl group) G3X theory predicts $D_0 = 351$ kJ mol^{-1} and CCSD predicts $D_0 = 377$ kJ mol^{-1}. Homolysis of the 1,2-bond of MTMB to give *t*BuCMeOMe$^\bullet$ (2-methoxy-3,3-dimethylbutyl radical) corresponds to 0 K bond dissociation energies of $D_0 = 335$ kJ mol^{-1} at G3X and $D_0 = 365$ kJ mol^{-1} at CCSD. Despite the fact that the D_0 values vary markedly between CCSD and G3X, both levels of theory estimate that the α-cleavage of methyl is less endothermic for MTMB than for MTBE (by 12 and 16 kJ mol^{-1}, respectively), as would be expected on the basis of steric hindrance.

While G3X calculations confirm the expectation that the 2,3-bond of MTMB is the one most easily cleaved, this level of theory gives calculated D_0 values for the two possible α-cleavages that are closer together than might have been anticipated. If the acti-

Table 2

DFT electronic energies (a.u.), unscaled zero point energies (kJ mol^{-1}), G3X energies (a.u.), and CCSD energies (a.u.) of HME, MTMB, MTBE, and their homolysis fragments using geometries optimized at B3LYP/6-31G(2df,p)

Formula	Abbreviated	B3LYP	ZPE	G3X (0 K)	CCSD
(CH$_3$)$_3$CC(CH$_3$)$_3$	HME	−315.729545	639	−315.359376	−314.905854
(CH$_3$)$_3$CC(CH$_3$)$_2$OCH$_3$	MTMB	−390.941418	650	−390.533186	−389.973150
(CH$_3$)$_3$COCH$_3$	MTBE	−272.998803	428	−272.717508	−272.330985
(CH$_3$)$_3$C radical	*t*Bu$^\bullet$	−157.812298	305	−157.616387	−157.387834
(CH$_3$)$_2$COCH$_3$ radical	MeOCMe$^\bullet$	−233.023958	320	−232.790851	−232.455274
CH$_3$ radical	Me$^\bullet$	−39.8433562	78	−39.792981	−39.720503
(CH$_3$)$_3$CC(CH$_3$)OCH$_3$ radical	*t*BuCMeOMe$^\bullet$	−350.972148	542	−350.612575	−350.102174
(CH$_3$)$_2$CC(CH$_3$)$_2$OCH$_3$ radical	MeOCMe$_2$CMe$_2^\bullet$	−350.965188	539	−350.608212	

vation energies for 1,2-bond homolysis and 2,3-bond homolysis of MTMB were truly separated by only 5 kJ mol^{-1}, m/z 18 (from photoionization of CD_3 radicals) should have been observed in Fig. 2 with an intensity roughly one-half that of m/z 15. Since m/z 18 is barely detectable, either the activation barriers are much further apart than the calculated G3X difference in D_0 values, or else the Arrhenius preexponential factors differ greatly.

The D_0 values calculated at CCSD/6-31G(2df,p)//B3LYP/6-31G(2df,p) using single and double excitations differ markedly from those at G3X. The 0 K dissociation energy of the 2,3-bond of MTMB has a value of $D_0 = 316$ kJ mol^{-1}, while the calculated value for the 1,2-bond is $D_0 = 365$ kJ mol^{-1}. In other words, CCSD gives a difference in D_0 (49 kJ mol^{-1}) that is more consistent with the experimental results reported here.

5. Discussion

When the hydrocarbon mixture used as a motor fuel autoignites in an automobile cylinder, engine knock results, and it becomes necessary to add antiknock agents. The two most prevalent antiknock compounds used in the 20th century, tetraethyllead and MTBE, have now been banned in many locales, the former on the basis of its toxicity and the latter because of its solubility in water. Other methyl *tert*-alkyl ethers (higher homologues of MTBE) also exhibit antiknock properties. Table 1 summarizes the decrease in water solubility with increasing carbon number, the qualitative trend that one would expect. The biggest jump occurs in going from *tert*-hexyl methyl ether (MDMB) to the title compound, MTMB.

The antiknock properties of alkyl ethers have been ascribed to their facile molecular elimination of alcohol. It has been hypothesized that the resulting alkenes inhibit radical chain reactions in the fuel/air mixture on the uncombusted side of the advancing flame front [25]. Hydrogen atom abstraction produces allylic radicals, which are thought to be less reactive in initiating ignition. Consistent with this model, a variety of fuel oxygenates with easily abstracted hydrogens, including 2-methylfuran, furfuryl alcohol, and *p*-cresol [26] are among the candidates proposed as viable antiknock additives, in addition to simple aliphatic alcohols [27], as well as the *tert*-alkyl ethers TAME [1], TOME [2,3], MDMB [6], ethyl *tert*-butyl ether (ETBE), and isopropyl *tert*-butyl ether (IPTBE) [28].

If this model is correct, the pyrolysis/supersonic jet expansion/118.2 nm photoionization TOF mass spectroscopic experiments reported here imply that MTMB ought to be a poor antiknock agent. Unlike MTBE or TOME, MTMB tends to produce free radicals under pyrolysis conditions, in preference to molecular elimination. Many potential fuel additives have been explored and found to be proknock [2]. The propensity of MTMB to undergo the homolysis drawn in Scheme 2 suggests that it may belong to this category.

The homolysis of MTMB appears to be highly specific for the 2,3-bond, yielding *tert*-butyl and methyl radicals, along with acetone-d_6. No cleavage of the 1,2-bond is seen, as attested by the virtual absence of CD_3^+ (m/z 18) in the photoionization mass spectra. The very tiny amount of m/z 18 that can be seen at

the highest temperature in Fig. 2 can be ascribed to thermal dissociation of acetone-d_6 under the pyrolysis conditions.

The choice of carrier gas affects the pyrolytic pathways observed in the present experiments. The longer contact time provided by argon allows lower temperature decompositions to be seen. Comparison of Fig. 1 with Fig. 3B shows that MTMB and MTBE exhibit similar propensities for molecular elimination below 900 K, where not much bond homolysis is seen. At temperatures $\geq$900 K, however, homolysis of the central bond of MTMB overtakes molecular elimination as the predominant pathway. The shorter contact time achieved using helium as carrier gas allows the homolysis products (methyl radical, acetone, and *tert*-butyl radical) to be detected. A shorter contact time has the advantage that subsequent dissociations of these products can be minimized.

Three levels of computation have been compared, which make very different predictions regarding bond homolyses. G3X theory gives dissociation energies for the 1,2- and 2,3-bonds of MTMB that are so close to one another that, if correct, CD_3 radicals ought to have been seen in the pyrolysis of MTMB-d_6. By contrast, CCSD calculations predict that the D_0 values differ by 49 kJ mol^{-1}, in agreement with the experimental observation that only the 2,3-bond cleaves.

6. Conclusions

The results of the experiments presented here lead to the following conclusions:

(1) With argon as carrier gas, MTMB and MTBE display comparable levels of molecular elimination of methanol at up to 875 K.
(2) With helium as carrier gas, MTMB exhibits homolytic cleavage of the 2,3-bond to a much greater extent than molecular elimination at temperatures $\geq$875 K.
(3) With helium as carrier gas, homolysis of the 2,3-bond of MTMB takes place with no competition from homolysis of the 1,2-bond in the temperature domain 875–950 K.

Acknowledgments

References

[1] A.F. Diaz, D.L. Drogos (Eds.), Oxygenates in Gasoline: Environmental Aspects, American Chemical Society (Oxford University Press), Washington, DC, 1979.

[2] M.J. Papachristos, J. Swithenbank, G.H. Priestman, S. Stournas, P. Polysis, E. Lois, J. Inst. Energy 64 (1991) 113.

[3] L.K. Rihko-Struckmann, R.S. Karinen, A.O.I. Krause, K. Jakobsson, J.R. Aittamaa, Chem. Eng. Process. 43 (2004) 57.

[4] L.K. Rihko, A.O.I. Krause, Ind. Eng. Chem. Res. 35 (1996) 2500.

[5] J. Liu, S. Wang, J.A. Guin, Fuel Process. Technol. 69 (2001) 205.

[6] D.E. Hendrickson, U.S. Patent Application WO9516763 (1995).

[7] L.A. Smith, Jr., H.M. Putman, H.J. Semerak, C.S. Crossland, U.S. Patent 6,583,325 (2003).

[8] T. Evans, K.R. Edlund, U.S. Patent 2,010,356 (1935).

[9] J. Ignatius, H. Jaervelin, P. Lindqvist, Hydrocarbon Process. 74 (2) (1995) 51.

[10] S. Hoogasian, C.H. Bushweller, W.G. Anderson, G. Kingsley, J. Phys. Chem. 80 (1976) 643.

[11] J.C. Traeger, T.H. Morton, J. Phys. Chem. A 109 (2005) 10467.

[12] L.F. Fieser, M. Fieser, Advanced Organic Chemistry, Reinhold Publishing, New York, 1961, p. 249.

[13] J.A. Walker, W. Tsang, Int. J. Chem. Kinet. 11 (1979) 867.

[14] H. Birkhofer, H.-D. Beckhaus, C. Rüchardt, Chem. Ber. 126 (1993) 1023.

[15] H.W. Biermann, G.W. Harris, J.N. Pitts Jr., J. Phys. Chem. 86 (1982) 2958.

[16] S.D. Chambreau, J. Zhang, J.C. Traeger, T.H. Morton, Int. J. Mass Spectrom. 199 (2000) 17.

[17] J.E. Taylor, D.A. Hutchings, K.J. Frech, J. Am. Chem. Soc. 91 (1969) 2215.

[18] V.D. Knyazev, I.A. Dubinsky, I.R. Slagle, D. Gutman, J. Phys. Chem. 98 (1994) 5279.

[19] D.W. Kohn, H. Clauberg, P. Chen, Rev. Sci. Instrum. 63 (1992) 4003.

[20] H. Clauberg, D.W. Minsek, P. Chen, J. Am. Chem. Soc. 114 (1992) 99.

[21] http://webbook.nist.gov/chemistry.

[22] L. Curtiss, P.C. Redfern, K. Raghavachari, J.A. Pople, Chem. Phys. Lett. 359 (2002) 390.

[23] L. Curtiss, K. Raghavachari, Theor. Chem. Acc. 108 (2002) 61.

[24] J.B. Pedley, R.D. Naylor, S.P. Kirby, Thermochemical Data of Organic Compounds, 2nd ed., Chapman and Hall, New York, 1986.

[25] A. Goldaniga, T. Faravelli, E. Ranzi, P. Dagaut, M. Cathonnet, Proceedings of the 27th Symposium on Combustion, 1998, p. 353.

[26] S. Gouli, E. Lois, S. Stournas, Energy Fuels 12 (1998) 918.

[27] W.J. Piel, Fuel Reformulation 4 (2) (1994) 28.

[28] J.F. Knifton, P.-S.E. Dai, J.M. Walsh, J. Chem. Soc., Chem. Commun. (1999) 1521.

[29] A. Fischer, M. Muller, J. Klasmeier, Chemosphere 54 (2004) 689.

[30] R.M. Stephenson, J. Chem. Eng. Data 37 (1992) 80.